Neutralizing breadth of antibodies targeting diverse conserved epitopes between SARS-CoV and SARS-CoV-2

Hua-Long Xiong
National Institute of Diagnostics and Vaccine Development in Infectious Diseases, School of Public Health & School of Life Science, Xiamen University

Hui Sun
Xiamen University

Si-Ling Wang
Xiamen University

Lunzhi Yuan
School of Public Health, Xiamen University, Xiamen, PR China.

Liqin Liu
Xiamen University

Yuhe Zhu
Xiamen University

Jinlei Zhang
Xiamen University

Yang Huang
Xiamen University

Ruoyao Qi
Xiamen University

Yao Jiang
Xiamen University

Jian Ma
Xiamen University

Min Zhou
Xiamen University

Yue Ma
Xiamen University

Rao Fu
Xiamen University

Siping Yan
Xiamen University

Mingxi Yue
State Key Laboratory of Molecular Vaccinology and Molecular Diagnostics, School of Life Sciences, Xiamen University
Yangtao Wu
State Key Laboratory of Molecular Vaccinology and Molecular Diagnostics, National Institute of Diagnostics and Vaccine Development in Infectious Diseases, School of Public Health, Xiamen University
Min Wei
Xiamen University
Yi-Zhen Wang
Xiamen University
Tingting Li
Xiamen University https://orcid.org/0000-0002-9917-7804
Yingbin Wang
State Key Laboratory of Molecular Vaccinology and Molecular Diagnostics, School of Life Sciences, School of Public Health, Xiamen University, Xiamen, 361102
Zi-Zheng Zheng
Xiamen University https://orcid.org/0000-0003-0099-4212
Hai Yu
State Key Laboratory of Molecular Vaccinology and Molecular Diagnostics, School of Life Sciences, Xiamen University, Xiamen
Tong Cheng
Xiamen University https://orcid.org/0000-0002-1638-6214
Shaowei Li
Xiamen University https://orcid.org/0000-0002-3374-1038
Quan Yuan
Xiamen University https://orcid.org/0000-0001-5487-561X
Jun Zhang
Xiamen University https://orcid.org/0000-0002-6601-9180
Yi Guan
Shantou University Medical College
Qingbing Zheng
Xiamen University https://orcid.org/0000-0002-7516-9965
Tianying Zhang
Xiamen University
Ningshao Xia (✉ nsxia@xmu.edu.cn)
Xiamen University https://orcid.org/0000-0003-0179-5266

Article

Keywords:

Posted Date: February 24th, 2022

DOI: https://doi.org/10.21203/rs.3.rs-1386044/v1

Neutralizing breadth of antibodies targeting diverse conserved epitopes between SARS-CoV and SARS-CoV-2

Hualong Xiong[1, #], Hui Sun[1, #], Siling Wang[1, #], Lunzhi Yuan[1, #], Liqin Liu[1, #], Yuhe Zhu[1, #], Jinlei Zhang[1, #], Yang Huang[1], Ruoyao Qi[1], Yao Jiang[1], Jian Ma[1], Ming Zhou[1], Yue Ma[1], Rao Fu[1], Siping Yan[1], Mingxi Yue[1], Yangtao Wu[1], Min Wei[1], Yizhen Wang[1], Tingting Li[1], Yingbin Wang[1], Zizheng Zheng[1], Hai Yu[1], Tong Cheng[1], Shaowei Li[1, *], Quan Yuan[1, 4, *], Jun Zhang[1, *], Yi Guan[3, 4, *], Qingbing Zheng[1, *], Tianying Zhang[1, *], Ningshao Xia[1, 2, *]

[1] State Key Laboratory of Molecular Vaccinology and Molecular Diagnostics; National Institute of Diagnostics and Vaccine Development in Infectious Diseases, School of Public Health, School of Life Sciences, Xiamen University, Xiamen 361102, China

[2] Research Unit of Frontier Technology of Structural Vaccinology, Chinese Academy of Medical Sciences, Xiamen 361102, China

[3] State Key Laboratory of Emerging Infectious Diseases, University of Hong Kong, Hong Kong 999077, China.

[4] Guangdong-Hongkong Joint Laboratory of Emerging Infectious Diseases/Joint Laboratory for International Collaboration in Virology and Emerging Infectious Diseases, Joint Institute of Virology (Shantou University and University of Hong Kong), Shantou University, Shantou 515063, China.

* Corresponding authors: shaowei@xmu.edu.cn (S.L.), yuanquan@xmu.edu.cn (Q.Y.), zhangj@xmu.edu.cn (J.Z.), yguan@hku.hk (Y.G.), abing0811@xmu.edu.cn (Q.Z.), zhangtianying@xmu.edu.cn (T.Z.), nsxia@xmu.edu.cn (N.X.)

# These authors contributed equally.

Abstract:

Antibody therapeutics for the treatment of COVID-19 has been highly successful while faces a challenge of the recent emergence of the Omicron variant which escapes the majority of existing SARS-CoV-2 neutralizing antibodies (nAbs). Here, we successfully generated a panel of SARS-CoV-2/SARS-CoV cross-neutralizing antibodies by sequential immunization of the two pseudoviruses. Of which, nAbs X01, X10 and X17 showed broadly neutralizing breadths against most variants of concern (VOCs) and X17 was further identified as a Class 5 nAb with undiminished neutralization against the Omicron variant. Cryo-EM structures of three-antibody in complex with the spike proteins of prototyped SARS-CoV-2, Delta, Omicron and SARS-CoV defined three non-overlapping conserved epitopes on the receptor-binding domain (RBD). The triple antibody cocktail exhibited enhanced resistance to viral escape and effective protection against the infection of Beta variant in hamsters. Our finding will aid the development of both antibody therapeutics and broad vaccines against SARS-CoV-2 and emerging variants.

Introduction

As of January 2022, the coronavirus disease 2019 (COVID-19) pandemic, caused by the severe acute respiratory syndrome coronavirus 2 (SARS-CoV-2) has resulted in over 5 million deaths worldwide[1-3]. Monoclonal antibodies (mAbs) isolated from SARS-CoV-2 infected individuals have exhibited effectiveness as both therapeutics or prophylactics against SARS-CoV-2[4-6], thus many neutralizing antibodies (nAbs), e.g. sotrovimab[7] and bamlanivimab[8] and nAb cocktails, e.g. casirivimab-imdevimab[9] and bamlanivimab-etesevimab[10] have been in Emergency Use Authorization (EUA) for treatment of COVID-19 in patients. However, constant evolution and genetic drift of SARS-CoV-2 has resulted in the emergence of many variants of concern (VOCs), including Alpha (B.1.1.7), Beta (B.1.351), Gamma (B.1.1.28), Delta (B.1.617.2) and Omicron (B.1.1.529) variants, the latter become the major concern of multiple countermeasures depending on the main protein of SARS-CoV-2 prototype strain. Shockingly, the Omicron variant accumulates a lot of residue substitutions in the spike (S) protein, of which 15 mutations are highly intertwined with common neutralizing epitopes in the receptor-binding domain (RBD)[11,12]. As reported, some critical mutations of SARS-CoV-2 VOCs could destroy the neutralization of mAbs potently neutralizing ancestral isolate, revealing that the protective efficacy of antibody therapeutics might be diminished[13-20]. Therefore, it is urgently required for nAbs with broader neutralizing breadth against current VOCs and future emerging variants.

The trimeric S protein mediates SARS-CoV-2 entry into host cells by the RBD that binds to the angiotensin-converting enzyme 2 (ACE2) receptor[1,21,22]. Since RBD is a

64 critical trigger factor inducing SARS-CoV-2 infection, thus has been identified as the
65 main target for therapeutics and vaccine development against COVID-19. A large
66 number of potently neutralizing mAbs have been identified which mainly target the
67 receptor-binding motif (RBM) on the RBD to efficiently inhibit S protein binding to
68 ACE2[4,23,24]. However, mutant residues of VOCs usually reside in the RBM, significantly
69 reducing the neutralization breadth of mAbs recognizing this site[13-18,25]. Nevertheless,
70 of all five identified classes of RBD-targeting nAbs[4,26], three classes, represented by
71 S309[27], S2X259[28] and S2H97[29], have been shown to cross neutralize SARS-CoV-2
72 and SARS-CoV, and further inhibit infection of most VOCs, revealing that epitopes
73 within these sites are highly conserved among *Sarbecoviruses*. Antibody cocktail
74 composed of representative nAbs binding to these conserved epitopes possibly have
75 the potential to prevent SARS-CoV-2 variants and spillover SARS-like virus.
76 Additionally, under pressure screening of antibody therapeutics, the emergence of
77 escape mutation becomes an important issue to be considered. Escape studies *in vitro*
78 have strongly supported the rationale of antibody cocktails consisting of noncompeting
79 antibodies to avoid resistance[13,15,30].

80 Previously reported nAbs are mainly obtained from human humoral immune
81 response induced by vaccination or natural infection of SARS-CoV or SARS-CoV-2.
82 The temporary exposure of single *Sarbecoviruses* hinders the generation of cross-
83 neutralizing mAbs[27-29]. Based on the experience of influenza virus research[31-33],
84 combination immunization of SARS-CoV and SARS-CoV-2 in sequence may play an
85 important role in the immune-focusing on the conserved epitopes to develop cross-

neutralizing antibodies.

In this study, we focus on the conserved epitopes between SARS-CoV-2 and SARS-CoV, generate a panel of broad neutralizing antibodies (bnAbs) against SARS-CoV, SARS-CoV-2 and VOCs from sequential immunized mice. Three representative bnAbs, X01, X10 and X17, are further identified potently cross-neutralize most VOCs but with decreased neutralization against Omicron in vary degree. High-resolution cryo-electron microscopy (cryo-EM) structures reveal three non-overlapped conserved epitopes and define the structural basis for the neutralization breadths of three bnAbs. Furthermore, the triple antibody efficiently resists to viral escape and protects Syrian hamsters against SARS-CoV-2 Beta variant challenge. Thus, our results expand the therapeutics strategy, based on conserved epitopes, to cope with circulating and future emerging SARS-CoV-2 VOCs and even spillover of SARS-like virus, and highlight the potential of diverse conserved epitopes in vaccine design.

Results

Sequential immunization of SARS-CoV and SARS-CoV-2 elicits cross-neutralizing antibodies

To efficiently generate SARS-CoV-2 and SARS-CoV cross-neutralizing mAbs targeting RBD, we implemented SARS-CoV and SARS-CoV-2 S proteins which were carried on recombinant vesicular stomatitis virus (VSV) pseudovirus, termed as rVSV-SARS and rVSV-SARS2, respectively, as previously reported[34]. The mice were alternately immunized with these two purified pseudoviruses at a one-week interval, of which

rVSV-SARS acted as the priming immunogen (**Fig. S1**). After three doses of both rVSV-SARS and rVSV-SARS2, the sequential immunized mice were sacrificed to build the hybridoma cell pools for the selection of cross-neutralizing mAbs against SARS-CoV and SARS-CoV-2. Finally, a total of 34 cross-neutralizing mAbs were obtained for further evaluation.

According to the diversity of the neutralization against SARS-CoV and SARS-CoV-2, 34 cross-neutralizing mAbs were further classified into 3 classes, termed as C1, C2 and C3 (**Fig. 1A** and **Table S1**). A majority of mAbs (19 of 34) were classified into C1, which showed comparable neutralizing efficacies against SARS-CoV-2 and SARS-CoV with half-maximal inhibitory concentration (IC_{50}) values differed within one order of magnitude, revealing that these cross-neutralizing mAbs recognize epitopes highly conserved within SARS-CoV-2 and SARS-CoV. Conversely, C2 and C3 contain weak cross-neutralizing mAbs with biased neutralization potencies against SARS-CoV and SARS-CoV-2, respectively (**Fig. 1B**, **C** and **Table S1**). We next determined the broadly neutralizing potencies of those mAbs against pseudoviruses of VOCs including B.1.1.7 (Alpha), B.1.351 (Beta), B.1.1.28 (Gamma), and B.1.617.2 (Delta). Of note, the cross-neutralizing mAbs in C1 showed comparable neutralizing efficacies against pseudoviruses of VOCs when compared to D614G (**Fig. 1B,** left panel), with IC_{50} values differing within one order of magnitude (**Fig. 1C,** left panel). These results indicated that nAbs in C1 not only ensure strong neutralization activities, but also effectively avoid the escape of SARS-CoV-2 variants. In contrast, mAbs in C2 showed limited neutralizing potencies to SARS-CoV-2 and VOCs (**Fig. 1B** and **C**, middle

panels), and SARS-CoV-2 biased nAbs in C3, although with better neutralizing efficacies against SARS-CoV-2 (**Fig. 1B**, right panel), showed less resist to VOCs (**Fig. 1C**, right panel), comparing to those nAbs in C1.

According to the above information, it is inferred that nAbs in C1 might be resistant to a variety of mutations found in VOCs as well as VOIs. To this end, we sought to investigate the single mutations on RBD for their influence on mAbs neutralization. A total of 55 RBD single-point mutations with high frequency since the COVID-19 outbreak were included in this study. Then, a set of corresponding 55 mutant SARS-CoV-2 pseudoviruses carrying these single-point mutations were constructed to evaluate all three classes of nAbs. Neutralization results were similar to that assessed against VOCs. Of these 3 class nAbs, C1 nAbs resistant to all mutations were identified as broad neutralizers, however, C3 nAbs with biased neutralization to SARS-CoV-2 showed a reduction of neutralization potencies against mutations in vary degrees (**Fig. 1D**). Of interesting, the antigenic site consisting of 470-490 residues (Site 470-490) was determined as a hit area of C3 nAbs since single mutations within this site significantly decreased the neutralizing activities (**Fig. 1D** and **Fig. S2**). The sensitivity of C3 nAbs to E484 residue might cause the diminished neutralization against Beta and Gamma variants. Additionally, there is a substitution of isoleucine for SARS-CoV to phenylalanine for SARS-CoV-2 at position 486 of RBD, the F486I mutation of SARS-CoV-2 RBD resulted in the abolish of neutralization of 7 of 11 C3 nAbs (**Fig. 1D** and **Fig. S2**), indicating residue 486 play critical role in medicating antigenic diversity between SARS-CoV-2 and SARS-CoV. Taken together, the sequential immunization

with SARS-CoV and SARS-CoV-2 successfully elicits cross-neutralizing antibodies which are also resistant to all VOCs emerged before Omicron. In addition, the epitopes recognized by C1 nAbs were valuable for deep exploration.

Cross-neutralizing antibodies belong to three clusters with different resistance to the Omicron variant

Since the potently broad neutralization of C1 mAbs, it is worthwhile to characterize their function in detail. To this end, an RBD-based competitive binding assay was carried out and those cross-neutralizing antibodies in the C1 class were further divided into three clusters (**Fig. 1E**). Of all these three clusters of nAbs, representative nAb X17 in Cluster 1 could not block the binding of receptor ACE2 on spike protein, while Cluster 2 and 3 nAbs, represented by X10 and X01, respectively, effectively blocked the binding of ACE2 (**Fig. S3**). These results suggested that the three clusters of nAbs may recognize three non-overlapping sites on RBD and the epitopes of X01 (Cluster 3) and X10 (Cluster 2) may overlap to the binding site of ACE2. In addition, the three representative nAbs were determined as potent cross-neutralizing antibodies against both SARS-CoV and SARS-CoV-2 with IC_{50} values less than 0.1 μg/mL. Remarkedly, X01 showed excellent neutralization, probably due to its effective blocking potency against ACE2 binding (The half-maximal effective concentration (EC_{50}): 0.17 μg/mL) (**Fig. S3**).

We then confirmed the broadly neutralizing efficacies of three representative nAbs against SARS-CoV-2 VOCs including the Omicron variant. X01 and X10 showed

potent neutralizing activities with IC_{50} ranging from 0.04 to 0.16 μg/mL against those VOCs raised between Omicron, which are significantly higher than that of X17 (IC_{50} ranging from 0.63 to 1.59 μg/mL) (**Fig. 1F**). Synchronously, we noted that no point mutations could destroy their neutralization activities, or even reduce IC_{50} within 10-fold, which further demonstrated the broad neutralizing activities of these three nAbs (**Fig. 1D**).

The currently dominant VOC, Omicron, which contains unprecedented 15 mutations in RBD, has been shown to be highly resistant to neutralization by plasma from vaccinated individuals, convalescent sera, and most reported neutralizing antibodies (nAbs)[11,12]. We next tested whether cross-neutralizing nAbs X01, X10 and X17 could also potently neutralize Omicron variant. Unfortunately, X01 and X10 remained only weak binding activities against Omicron spike protein with a half-maximal effective concentration (EC_{50}) of 3.29 and 18.79 μg/mL, respectively. In contrast, X17 still maintained strong interaction with the Omicron spike with an EC_{50} value of 0.005 μg/mL (**Fig. 1G**). Consistently, X17 showed comparable low neutralizing efficacy (IC_{50} 3.52 μg/mL) when compared to WT and other VOCs, while X01 and X10 almost lost their neutralizing activities against the Omicron variant (with IC50 of 49.70 and 50.16 μg/mL, respectively). Taken together, the antigenic mutations of the Omicron variant destroyed the neutralizing breadths of nAbs X01 and X10 but not X17.

Cross-neutralizing antibodies define three non-overlapping conserved epitopes on RBD

196 To define the conserved epitopes of the three cross-neutralizing antibodies, we first
197 employed the cryo-EM approach to determine the complex structures of three nAbs
198 combination binding to wild-type spike proteins SARS-CoV-2 (SARS-CoV-2-S) and
199 SARS-CoV (SARS-CoV-S), respectively. Cryo-EM structures of SARS-CoV-2-S and
200 SARS-CoV-S in complex with three nAbs simultaneously were obtained at resolutions
201 of 3.48 Å (**Fig. 2A-D, Fig. S4** and **8, Table S2**) and 3.83 Å (**Fig.2E-G, Fig. S5** and **8,**
202 **Table S2**), respectively. Of interesting, simultaneously binding of three nAbs to SARS-
203 CoV-2-S induced the dissociation of trimeric spike and we finally obtained the structure
204 of monomeric spike protein in complex with three nAbs (SARS-CoV-2-S:X01:X10:X17)
205 (**Fig. S4**). Superimposition of the atomic model of SARS-CoV-2-S:X01:X10:X17 onto
206 the structure of trimeric spike showed conspicuous antibody-induced steric clashes
207 mediated by both X10 and X17 but not X01, suggesting X10 and X17 may harbor
208 dissociation potency toward spike trimer (**Fig. 2C**). Furthermore, the binding of X01
209 and X10, but not X17, will occupy the space required for ACE2 binding (**Fig. 2D**),
210 therefore blocking the binding of ACE2 effectively (**Fig. S3**). As for SARS-CoV-
211 S:X01:X10:X17 reconstruction, both trimeric (~49%) and dissociated monomer S (~6%)
212 in complex with three nAbs were classified out (**Fig. S5**), suggesting the less potent
213 dissociation efficacy of nAbs on SARS-CoV-S when compared to SARS-CoV-2-S. The
214 particles of trimeric S complexes were selected for further reconstruction (**Fig. S5**). In
215 the 3.74 Å structure of trimeric SARS-CoV-S:X10:X01:X 17, all three RBDs of the spike
216 are in the “up” conformations and bound by three Fabs simultaneously, but only one
217 RBD was saturated bound (**Fig. 2G**), which was further reconstructed by localized

refinement to push local resolution (**Fig. 2E** and **Fig. S5**). Of note, three RBDs on nAb-bound SARS-CoV-S are raised in extremely open states with degrees (compared to close RBD) ranging from 85 to 87°, compared to about 42° for the normal open RBD in spike protein (**Fig. 2H**), suggesting that only enough opened RBDs can accommodate three Fabs especially for X10 and X17 to avoid steric clashes and to diminish the disruption of trimeric spike.

We next investigated the simultaneously binding potential of three nAbs to spike proteins of Delta (Delta-S) and Omicron (Omicron-S) variants, respectively. Similar to SARS-CoV-S, the binding of three nAbs on Delta-S induced partial dissociation of trimeric spike (**Fig. S6**) and we obtained the structures of trimeric Delta-S:X01:X10:X17 at resolutions of 3.54 Å (global refinement) and further performed localized refinement focused on the interface and achieved a structure at 3.77 Å resolution (**Fig. 2I-K, Fig. S6** and **8, Table S2**). As for the Omicron variant, although X01 and X10 showed significantly decreased efficacies in both the binding and neutralizing assays (**Fig. 1G** and **H**), we still could obtain a medium resolution (6.56 Å) structure of immune complex Omicron-S:X01:X10:X17 (**Fig. 2L**, **Fig. S7** and **8**, **Table S2**).

The footprints of X01, X10 and X17 contain 18, 21 and 16 RBD residues respectively, and only the X10 footprint is found to partially overlap with the ACE2-binding site (Y449, Q493) **(Fig. 2M-O)**. The footprints of three nAbs are dramatically non-overlapped between each other and therefore allow the simultaneous binding of three nAbs to RBD (**Fig. 2M-P**). Furthermore, the footprint of X17 excluded all of the VOCs and VOIs mutations (**Fig. 2O-Q**), and the footprints of X10 and X01 contain only

4 (N440, L452, E484, Q493) and 2 (S371, S375) VOCs mutation sites, respectively (**Fig. 2M** and **N**), suggesting their highly conserved epitopes among SARS-CoV-2 VOCs, in particular for that of X17.

Structural basis for the broad neutralization of nAbs against VOCs

We next analyzed the interaction details of three nAbs to SARS-CoV-2 WT, Delta and SARS-CoV RBDs, respectively. The epitope of X10 in WT RBD composes of 21 residues, including 10 residues (R346, Y351, T345, N440, L441, D442, K444, Y449, N450, T470 and Q493) which form an extensive interaction network containing 15 hydrogen bonds and 1 salt bridges **(Fig. 2M, Fig. 3A** and **B)**. Although X10 epitope contains VOC mutation site L452 (**Fig. 2M**), it does not participate in hydrogen bond or salt bridge interaction to X10 (**Fig. 3B**), the L452R substitution in Delta-RBD not only with no influence on the binding of X10, but instead, the longer side chain of arginine forms additional hydrogen bonds with X10 (**Fig. S10B**), explaining why X10 confers more than 2-fold higher neutralization against Delta variant (IC_{50}: 42 ng/mL) than D614G strain (IC_{50}: 86 ng/mL) **(Fig. 1F** and **Table. S1)**. Additionally, 11 of 20 residues of the X10 epitope in SARS-CoV RBD are conserved among SARS-CoV-2 and SARS-CoV and the other 5 residues are substituted of similar amino acids **(Fig. 2Q** and **Fig. 3C)**. Consequently, the interactions between the heavy chain of X10 and SARS-CoV RBD are decreased to 3 hydrogen bonds in comparison with 7 hydrogen bonds and 1 salt bridge between X10 and SARS-CoV-2 RBD (**Fig. 3A** and **Fig. S10C**). In contrast, the interactions between the light chain of X10 and SARS-CoV RBD are

enhanced by providing more hydrogen bonds (9 versus 8) and salt bridges (1 versus 0) compared to that between X10 and SARS-CoV-2 RBD (**Fig. 3B** and **Fig. S10D**). Therefore, though X10 recognizes an epitope that is sequentially diverse between SARS-CoV-2 and SARS-CoV to a certain degree, it still enables it to effectively bind and neutralize SARS-CoV **(Fig. 1A** and **Table S1)**.

Another cross-neutralizing mAb, X01, recognizes a conserved epitope that is near the well-known CR3022 binding site[35] but a step closer to ACE2 binding site[36] (**Fig. 2N** and **Fig. S11**). Similar to X10, an elaborate interaction network containing 15 hydrogen bonds and 4 salt bridges between X01 and SASR-CoV-2 RBD occurs in the interface **(Fig. 3D** and **E)**. X01 also strongly interacts with Delta RBD and SARS-CoV RBD by providing similar hydrogen bonds and salt bridges interaction as that of WT-RBD (**Fig. S10E-H**). The epitope of X01 on SARS-CoV RBD comprises 17 residues compared to 18 residues in SARS-CoV-2 RBD, among which, 14 residues are completely conserved (**Fig. 2Q** and **Fig. 3F**), which accounts for the comparable neutralizing potencies of X01 against SARS-CoV and SARS-CoV-2 (**Fig. 1A** and **Table S1**).

X17 epitope locates at a cryptic site that is far away from the ACE2-binding site, resembles the reported S2H97[26,37] and 6D6/7D6[38] (**Fig. 2O** and **Fig. S11A**). X17 contacts WT RBD mainly using 9 residues (R355, R357, N394, Y396, D428, K462, F464, E516, H519) by forming an amount of 15 hydrogen bonds and 5 salt bridges (**Fig. 3G** and **H**). When binding to Delta RBD and SARS-CoV RBD, the key residues involved in interface interactions are almost unaltered (**Fig. S10I-L**). Specially, 14 of 16 residues of the epitope of X17 on SARS-CoV RBD are consistent with that of SARS-

CoV-2 RBD and the rest 2 residues are substituted by similar amino acid (R357K and K462R) (**Fig. 2Q** and **Fig. 3I**). In general, the epitopes of such nAbs that are categorized to Class 5 are highly conserved among *Sarbecoviruses* and spatially far from almost all the mutation sites of VOCs of SARS-CoV-2 including Omicron variant[26,37] **(Fig. 2O-Q, Fig. S11B)**. Thus, compared to X10 and X01, X17 is an optimal nAb with excellent binding activity to Omicron (EC_{50}: 0.005 μg/mL) although with unsatisfactory neutralization against Omicron (IC_{50}: 5.7 μg/mL) (**Fig. 1G** and **H**).

As for Omicron, VOC mutation sites E484, Q493 and N440 are involved in X10 interaction while S371 and S375 are involved in X01 interaction **(Fig. 2P** and **Fig. 3J)**. E484, Q493 and N440 on WT RBD provide appreciable contacts as well as 2 hydrogen bonds interaction with X10 **(Fig. 3K)**. Although single mutation of any of the three residues was shown not or slightly affect the binding of X10 (**Fig. 1D**), the synchronal mutation of which may induce the decrease of neutralization of X10 against Omicron. Also, S371 and S375 in WT RBD that included in X01 epitope, involve in appreciable interactions with X01 (**Fig. 3J** and **L**). S371 and especially S375 contribute multiple contacts as well as hydrogen bonds interactions between S371 and $Y105^{H}$, S375 and both $Y103^{H}$ and $Y105^{H}$ **(Fig. 3L)**. Therefore, the mutation of these residues causes the devastating decreased neutralizing activity of X01 against Omicron **(Fig. 1H).** Taken together, the combination of multiple mutations in Omicron RBD makes it easier to escape cross-neutralizing antibodies X10 and X01, as well as the majority of existing cross-neutralizing antibodies[11]. In contrast, considering the highly conserved epitope and broadly neutralizing breadth of Class 5 nAb X17, which may serve as an essential

306 component of the next-generation antibody cocktail therapeutics against various
307 SARS-CoV-2 variants in the future.
308
309 **Triple antibody cocktail resists viral escape *in vitro***
310 Several previous studies have reported that combination therapy of dual nAbs
311 targeting noncompeting RBD epitopes decreases rapid viral escape caused by
312 monotherapy[13,15,30]. To understand the escape characteristics of the SARS-CoV-2
313 under the pressure of each of or cocktail of three nAbs obtained in this study, we
314 performed *in vitro* escape selection experiments using a previously reported replicative
315 recombinant VSV expressing SARS-CoV-2 spike protein (rVSV-SARS2)[30] **(Fig. S12A)**.
316 Complete escape of rVSV-SARS2 resistant to X01 or X10 was rapidly selected by 3
317 passages **(Fig. S12B** and **C)**. In contrast, X17 could maintain the neutralizing activity
318 over 11 consecutive passages and the completely viral escape was raised at the 13th
319 passage (P13), suggesting that the Class 5 epitope is relatively more tolerant to
320 immunologic pressure **(Fig. S12B** and **C)**. Furthermore, the triple antibody cocktail
321 showed no viral escape even for 20 passages **(Fig. S12B** and **C)**. These results
322 indicated that the combination of three cross-neutralizing antibodies composed of X01,
323 X10 and X17 has the potential in preventing the rapid emergence of SARS-CoV2 viral
324 escape.
325
326 **Cross-neutralizing antibody cocktail efficiently protect hamsters from Beta**
327 **variant infection**

328 Considering the diverse epitopes, complementary neutralizing breadths and resistance
329 to viral escape of X10, X01 and X17, we subsequently evaluated the therapeutic
330 activity of triple antibody cocktail against infection of Bata variant (B.1.351) in Syrian
331 hamster model. Following the intranasal challenge of 1×10^4 plaque-forming units (PFU)
332 of B.1.351, antibody cocktail was intravenously administered at a single dose of total
333 35 mg/kg (each antibody at 11.7 mg/kg) at 1 day post-infection (dpi), then the
334 quantification of viral load and pathological analysis was carried out in the respiratory
335 tract at 5 dpi. Hamsters in the untreated group significantly lost body weight by an
336 average of 13.8% and 50% of which were sacrificed at 5 dpi (**Fig. 4A** and **B**). In
337 contrast, hamsters in the treated group showed a more constant weight level with only
338 2.3% loss and all survived at 5 dpi (**Fig. 4A** and **B**), suggesting the excellent
339 therapeutic efficiency of the triple antibody cocktails.

340 Next, the viral loads in lung tissues were measured to further evaluate the efficacy
341 of antibody cocktails in the inhibition of viral replication at 5 dpi. While the amounts of
342 viral RNA of the untreated group surged to about 1×10^9 copies/mL in lung tissues
343 including lung regions proximal (Lu1) and distal (Lu2) to the hilum, hamsters in the
344 antibody-treated group significantly inhibit virus replication by 2-3 order of magnitude
345 in reduction (**Fig. 4C**). Moreover, in the non-lung respiratory tract, such as nasal
346 turbinates (NT) and trachea (Tr), antibody-treated hamsters were also tested with a
347 significantly decreased viral load when compared to that of untreated hamsters (**Fig.**
348 **4C**). Viral infection-related lung damage was further evaluated. The treatment with
349 antibody cocktail can effectively inhibit the occurrence of multifocal diffuse hyperemia

and consolidation in gross observations of lung tissues, compared to the untreated group (**Fig. S13**). Additionally, histopathological examination documented that, compared to the untreated group, there were no significant lesions of alveolar epithelial cells and focal hemorrhage in the lung tissues of hamsters in antibody-treated group (**Fig. 4D** and **E**). The treatment with antibody cocktail can profoundly decrease the pathological severity scores to an average of 2.8, versus 10.7 for the untreated group (**Fig. 4F**). Collectively, these results revealed that the administration with a triple antibody cocktail can effectively protect hamsters against infection of Bata variant and infection-related lung damage.

Discussion:

The emerging SARS-CoV-2 variants of concern (VOCs), especially Omicron, showed increased transmissibility and resistance to antibody neutralization and further raised the requirement of broad antibody therapeutics and vaccines[11,12,39]. The recent withdrawal of bamlanivimab has demonstrated that the nAb epitopes located on or adjacent to the RBM under selection pressure are high mutant, and even a combination of two noncompeting nAbs (e.g. bamlanivimab/estevimab) could not prevent the reduction of neutralization potency against SARS-CoV-2 P.1 variant which emerged before Omicron variant[40,41]. It's known that RBD-specific antibodies can be categorized into at least five classes (Class 1~5) based on their binding modes and the competition with ACE2[26]. Many of reported nAbs from class 3, class 4 and class 5, represented by S309 [27], S2X259 [42], and S2H97[26,37], respectively (**Fig. S11B**), have

been demonstrated with broadly neutralizing breadths against many VOCs as well as SARS-CoV. However, most of above nAbs, including those authorized under EUA, decrease their neutralizing activities against Omicron[11,12,39,43,44]. Consistently, cross-neutralizing antibodies X01, X10 and X17 obtained in this study revealed decreased or limited neutralizing potencies against Omicron. According to the previous categorization information, nAbs X10, X01, and X17 could be classified into Class 3, Class 4, Class 5, respectively (**Fig. S11A**). Of note, the binding sites of those rare Class 5 nAbs, were previously revealed spatial cryptic and highly conserved among *Sarbecoviruses*. The epitope of X17 revealed in this study confirmed that the binding sites of those Class 5 nAbs are highly conserved between SARS-CoV-2 and SARS-CoV, and without any mutations of VOCs including Omicron. Unfortunately, the less potent neutralizing efficacies (IC_{50}: 1~10 μg/mL) of Class 5 nAbs including X17 may limit their potential for clinical application. To improve neutralization potency, modification of X17 volume to strongly block RBD attachment to ACE2 may be a potential optimization direction[45,46]. Nevertheless, the conserved and cryptal epitopes may serve as an ideal target for the development of next-generation broad vaccines against SARS-CoV-2 and variants.

Class C1 antibodies that potently neutralized SARS-CoV and SARS-CoV-2 as well as most VOCs were generated in abundance by sequential immunization with VSV-SARS and VSV-SARS2. We previously have demonstrated that the combined immunization of coronavirus spikes could also effectively elicit cross-neutralizing antibodies[38]. These information together demonstrate that sequential immunization

394 can produce cross-neutralizing antibodies targeting to more conserved antigenic sites.
395 The emergence of the Omicron variant substantially destroy the broad neutralization
396 of most previously reported nAbs that elicit from the infection or immunization of single
397 virus, e.g. SARS-CoV or SARS-CoV-2 prototype strain. Although the Omicron variant
398 generates a big mutational leap on RBD, sequential immunization with VSV-SARS and
399 VSV-SARS2 in this study was showed success to achieve efficient immune focus on
400 those most conserved epitopes, such as epitopes targeted by Class 5 antibodies.
401 However, the mutations of the Omicron variant residing in these conserved epitopes
402 for Class 3 and Class 4 nAbs caused a significant decrease in neutralization potencies.
403 The structural analysis revealed that the E484, Q493 and N440 mutations on Omicron
404 RBD may diminish the binding of Class 3 nAb X10. Based on the previous study, the
405 G446S mutation on Omicron RBD may also diminish the binding of another Class 3
406 nAb REGN10987[47]. As for Class 4 nAb X01, S371 and S375 mutations were found to
407 mediate the escape to the Omicron variant. A similar phenomenon may also occur in
408 H014 by which S371L may mediate the resistance of Omicron to it[48]. Considering the
409 unprecedented evasion from most nAbs and immune response of SARS-CoV-2
410 prototype strain, Omicron variant should become another important component of
411 sequential immunization, besides SARS-CoV and SARS-CoV-2, to achieve more
412 accurate immune focus, inducing bnAb response against current VOCs and emerging
413 variants in the future.

414 During the past two years, a large number of antibodies and antibody cocktails
415 have been developed to fight COVID-19. In this study, we evaluated the combination

of three cross-neutralizing nAbs against SARS-CoV-2 infection in animals for the first time. X01, X10 and X17 were identified to effectively protect against B.1.351 infection *in vivo*. A cocktail of three mAbs (atoltivimab, maftivimab, and odesivimab) combatting Ebola virus have been approved in 2020[49]. These results provide important insights into the feasibility for the development of a triple antibody cocktail against infectious diseases. Structure analyses revealed the existence of at least three noncompeting cross-neutralizing epitopes arraying around RBD. The simultaneously occupying of such epitopes, e.g. simultaneously binding of X01, X10 and X17, will shield the majority of the flank, therefore performing excellent or even synergetic neutralization against SARS-CoV-2 and variants. For this triple antibody cocktail, X01 and X10 moderately block RBD binding to ACE2 and confer potent neutralization (IC_{50}: 0.05-0.16 μg/mL) against SARS-CoV-2 and most VOCs mainly by interfering virus-receptor interaction. The third nAb X17, which recognized the highly conserved and cryptic epitope with an excellent binding affinity, buried in the lying down RBD similar to that CR3022-like antibodies50, may further neutralize virus by destabilization of spike protein. Furthermore, although less potent when compared to the of single nAbs against other VOCs, the triple antibody cocktail showed a synergetic neutralizing efficacy (IC_{50}: 3.5 μg/mL) against Omicron. Considering that the clinical administration antibody therapeutics always use an extremely large dosage, e.g. Trump received antibody treatment for COVID-19 with total dosage of 8 g[6]. The 3.5 μg/mL level of neutralization may also provide effective protection from Omicron infection, which will be confirmed in our further animal studies. Additionally, previous studies have demonstrated a higher

frequency of mutations in the RBM over the rest of the RBD[51]. The footprints of three nAbs are with no or few overlaps to the ACE2 binding site, which may further benefit in avoiding antibody-induced immune escape. Indeed, the absence of escape variants under the pressure of a single X17 further implies that escape mutations residing in the X17 epitope might destroy SARS-CoV-2 replication, possibly due to the important role of this epitope in the SARS-CoV-2 infection process. The triple antibody cocktail based on X17 provides stronger prevention against a selection of rapid escape viruses, resulting from the synergistic inhibition that is lacking for single antibody therapeutics. These results demonstrated that the triple antibody cocktail is a promising candidate for immunotherapy against pandemic SARS-CoV-2 VOCs.

In summary, the above results documented that sequential immunization could achieve immune focus on the conserved epitopes of SARS-CoV and SARS-CoV-2 to induce amounts of bnAbs against SARS-CoV, SARS-CoV-2 and VOCs. The combination of three representative bnAbs X01, X10 and X17 exhibited synergistic neutralizing activities, resistance to viral escape and protection of hamsters from disease caused by SARS-CoV-2. We also define the structural basis for neutralization breadth and potency by this triple antibody cocktail. This study suggests a new strategy for the development of antibody therapeutics as well as universal SARS-CoV-2 vaccines based on immune focus.

Methods

Ethics statement

460 The BALB/c mice were purchased from Shanghai SLAC Laboratory Animal Co.,
461 Ltd. Hamsters (LVG golden Syrian hamsters) were purchased from Charles River
462 Laboratories. All experiments with infectious SARS-CoV-2 were performed in the
463 biosafety level 3 (BSL-3) and animal biosafety level 3 (ABSL-3) facilities. The Golden
464 Syrian Hamster (Charles River Laboratories) was raised in specific pathogen-free
465 animal feeding facilities. All animal studies were carried out in strict accordance with
466 the recommendations of the Guide for the Care and Use of Laboratory Animals. The
467 mouse and hamster studies were conducted under the approval of the Institutional
468 Animal Care and Use Committee of Xiamen University. All the animal experiments
469 were approved by the Medical Ethics Committee (SUCM2021-112).

470 **Cell lines**

471 Vero-E6 (American Type Culture Collection [ATCC], CRL-1586), BHK21 (ATCC,
472 CCL-10), SP2/0 (ATCC), and 293T (kindly gifted by Dr. Jiahuai Han) cells were
473 maintained in high glucose DMEM (SIGMA-ALDRICH) supplemented with 10% FBS
474 (GIBCO), penicillin (100 IU/mL), streptomycin (100 μg/mL) in a 5% CO2 environment
475 at 37°C and passaged every 2 days. BHK21-hACE2 cell was developed by stable
476 transfection of hACE2-expressing plasmid following puromycin resistance selection.
477 All cell lines used in this study were routinely tested for mycoplasma and found to be
478 mycoplasma-free.

479 **Production of pseudoviruses**

480 Recombinant vesicular stomatitis virus (rVSV) expressing SARS-CoV
481 spike(GenBank: AY278554.2) (termed as rVSV-SARS), SARS-CoV-2 prototype strain

spike (GenBank: MN908947) (termed as rVSV-SARS2), SARS-CoV-2 VOCs spikes or 55 SARS-CoV-2 spikes with different single point mutations were generated as previously described[34]. Briefly, the spike gene of SARS-CoV or SARS-CoV-2 with a C-terminal 18 amino acids truncation was cloned into the eukaryotic expression plasmid pCAG (Addgene), respectively. rSARS-CoV and rSARS-CoV2 were rescued by VSVdG-EGFP-G (Addgene, 31842) from the Vero E6 cells transfected with plasmids pCAG-SARS1-Sdel18 and pCAG-SARS2-Sdel18[52], respectively. The supernatant was harvested and purified by Capto Core 700 (Cytiva) multimodal chromatography, the viral particles were collected in the column flowthrough.

Neutralization assay based on VSV pseudovirus

Neutralizing activities of antibodies against SARS-CoV, SARS-CoV-2, SARS-CoV-2 VOCs and SARS-CoV-2 with different single point mutations were quantified based on recombinant VSV as previously described[34], a series of diluted monoclonal antibodies were mixed with pseudoviruses carrying spike of SARS-CoV, SARS-CoV-2 or variants and incubated at 37℃ for 1 hour, respectively. Then the mixture was transferred to BHK21-hACE2 cells seeded in 96-well microplate. After 12 hours of incubation, fluorescence images were captured by Opera Phenix (PerkinElmer) and quantitatively analyzed by the Columbus system (PerkinElmer). The reduction percentage of EGFP in each well compared to the control wells was calculated. The IC_{50} value was determined by the 4-parameter logistic regression using GraphPad Prism (version 8.0.1).

Sequential immunization and cross-neutralizing antibody screening

BALB/c mice were immunized with purified rVSV-SARS and rVSV-SARS2 once a week, alternately. After six doses of immunization, mice were sacrificed and the spleen cells were harvested for cell fusion with mouse myeloma cell line SP2/0 to generate hybridomas. The pseudovirus neutralization assay based on rVSV-SARS and rVSV-SARS2 were used to screen the hybridomas secreting cross-neutralizing antibody against both SARS-CoV and SARS-CoV-2. The screening assay was described previously[34].

Blocking capacity of nAbs against ACE2 binding

Microplates pre-coated with recombinant antigens of RBD were provided by the Wantai BioPharm. Antibodies at 100 μg/mL, respectively, were five-fold serially diluted, added to the wells (100 μL), and incubated at 37°C for 0.5 h. ACE2-hFc (provided by the Wantai BioPharm) was diluted at 85 ng/mL in SD-1 (Wantai BioPharm), added to the wells (100 μL), and incubated at 37 °C for 0.5 h. Then wells were washed, A horseradish peroxidase (HRP)-labeled goat anti-human antibody (Abcam) was used as the secondary antibody at 1:5000 for 30 min. Wells were washed again and the reaction was catalyzed using o-phenylenediamine substrate at 37 °C for 10 min. The OD450 nm (reference, OD630nm) was measured on a microplate reader (TECAN, Männedorf, Switzerland) with a cut-off value of 0.1. The blocking capacity was measured quantitatively by comparing OD in the presence and absence of nAbs, and transformed using the formula [1- ($OD_{present}$/ OD_{absent})] x100%. and the blocking IC_{50} values were calculated by Prism software using non-linear regression (four parameters).

Competition binding assay

Briefly, the unlabeled nAbs (50 μg per well) or 20 mM phosphate-buffered saline (PBS) (GIBCO) were added to SARS-CoV-2 RBD-coated 96-well microplates and then incubated for 30 min at 37°C. Next, HRP-conjugated nAbs were added at selected dilutions, at which OD readings was ~1.5 present. After incubation for 30 min at 37°C, the microplates were rinsed and the color was developed. The blocking rate was measured quantitatively by comparing OD in the presence and absence of competitor mAbs, and transformed using the formula [1- ($OD_{present}$/ OD_{absent})] x100%.

Cryo-EM sample and data collection

Aliquots (3 μL) of 3.5 mg/mL mixtures of purified SARS-CoV-2 WT-S, Delta-S, Omicron-S proteins (Sino Biological Inc.) and SARS-CoV-S protein (Sino Biological Inc.) in complex with excess Fab fragments of three nAbs were incubated in 0.01% (v/v) Digitonin (Sigma) and then loaded onto glow-discharged (60 s at 20 mA) holey carbon Quantifoil grids (R1.2/1.3, 200 mesh, Quantifoil Micro Tools) using a Vitrobot Mark IV (ThermoFisher Scientific) at 100% humidity and 4°C. Data were acquired using the SerialEM software on an FEI Tecnai F30 transmission electron microscope (ThermoFisher Scientific) operated at 300 kV and equipped with a Gatan K3 direct detector. Images were recorded in the 36-frame movie mode at a nominal 39,000× magnification at super-resolution mode with a pixel size of 0.389 Å. The total electron dose was set to 60 e^{-} $Å^{-2}$ and the exposure time was 4.5 s.

Image processing and 3D reconstruction

Drift and beam-induced motion correction were performed with MotionCor2[53] to

produce a micrograph from each movie. Contrast transfer function (CTF) fitting and phase-shift estimation were conducted with Gctf[54]. Micrographs with astigmatism, obvious drift, or contamination were discarded before reconstruction. The following reconstruction procedures were performed by using Cryosparc V3 [55]. In brief, particles were automatically picked by using the “Blob picker” or “Template picker”. Several rounds of reference-free 2D classifications were performed and the selected good particles were then subjected to ab-initio reconstruction, heterogeneous refinement and final non-uniform refinement. The resolution of all density maps was determined by the gold-standard Fourier shell correlation curve, with a cutoff of 0.143[56]. Local map resolution was estimated with ResMap[57].

Atomic model building, refinement, and 3D visualization

The initial model of nAbs was generated from homology modeling by Accelrys Discovery Studio software (available from: URL: https://www.3dsbiovia.com). The structure of SARS-CoV-2 RBD and SARS-CoV RBD from the structure of WT trimeric spike (pdb no. 6VSB[58]) and SARS-CoV RBD in complex with CR3022 (pdb no. 7JN5[59]), respectively, were used as the initial modes of our WT-RBD,Delta-RBD and SARS-CoV RBD. We initially fitted the templates into the corresponding final cryo-EM maps using Chimera [60], and further corrected and adjusted them manually by real-space refinement in Coot[61]. The resulting models were then refined with phenix.real_space_refine in PHENIX[62]. These operations were executed iteratively until the problematic regions, Ramachandran outliers, and poor rotamers were either eliminated or moved to favored regions. The final atomic models were validated with

Molprobity[63,64]. All figures were generated with Chimera or ChimeraX[65,66].

The initial model of nAbs was generated from homology modeling by Accelrys Discovery Studio software (available from: URL: https://www.3dsbiovia.com). The structure of RBD from the structure of WT trimeric spike (pdb no. 6VSB[58]) was used as the initial modes of our WT-RBD and Omicron RBD. We initially fitted the templates into the corresponding final cryo-EM maps using Chimera[60], and further corrected and adjusted them manually by real-space refinement in Coot[61]. The resulting models were then refined with phenix.real_space_refine in PHENIX[62]. These operations were executed iteratively until the problematic regions, Ramachandran outliers, and poor rotamers were either eliminated or moved to favored regions. The final atomic models were validated with Molprobity[63,64]. All figures were generated with Chimera or ChimeraX [65,66].

Generation of replicative recombinant VSV-SARS2 virus

Replicative recombinant VSV-SARS2 (rrVSV-SARS2) was generated by replacing the VSV glycoprotein with the native SARS-CoV-2 spike protein from Wuhan-Hu-1 strain (GenBank: MN908947) with a C-terminal 18 amino acids truncation and encoding the GFP genes insert to 3' end of VSV genome. 293T cells were plated on Poly-L-lysine solution (SIGMA-ALDRICH) treated plates and incubated overnight in DMEM (SIGMA-ALDRICH) containing 10% fetal bovine serum (GIBCO) and 1% Penicillin/Streptomycin/L-glutamine (Invitrogen). The following day, the cells were infected by recombinant vaccinia virus producing the T7 RNA polymerase (rVV-T7) and transfected with the VSV genomic clone driven by a T7 promoter and helper plasmids

592 expressing the VSV-N, VSV-P, VSV-G, VSV-L with Lipofectamine LTX reagent
593 (Invitrogen). After 48 hours, the supernatant of transfected cells was co-cultured with
594 Vero E6 cells (ATCC) transfected with VSV-G. Cells were monitored for GFP
595 expression or cytopathic effect (CPE) indicative of virus replication. Virus was then
596 expanded and titered in BHK21-hACE2 cells. After collection, stocks of both viruses
597 were centrifuged at 3500 rpm for 5 minutes to clarify and frozen at −80°C.

598 ***In vitro* escape studies**

599 Escape studies were performed with rrVSV-SARS2 virus[30]. Viral escape was
600 selected by incubating rrVSV-SARS2 under antibody pressure ranging from 0.02
601 μg/mL to 20 μg/mL. After 60 minutes of incubation, the mixture was used to infect $1x10^6$
602 Vero E6 cells at a multiplicity of infection (MOI) of 1. Virus replication was monitored
603 by screening for GFP expression or cytopathic effect (CPE) over 96 hours. When >90%
604 cells were GFP-positive or exhibit 90-100% CPE, the supernatant was collected and
605 clarified by centrifugation. For subsequent rounds of selection, 100 μL of supernatant
606 containing the virus was passaged under the same or greater antibody concentrations
607 as in previous passages until complete CPE was observed after antibody treatment at
608 a concentration of $\geqslant$20 μg/mL. The consecutive passages virus was then expanded
609 and titered in BHK21-hACE2 cells. Neutralization assays of antibodies against the
610 virus consecutive passaged were made as previously described [34].

611 **Therapeutic effects against Beta variant in hamsters**

612 The therapeutic effects of cross-neutralizing antibodies cocktail against Beta
613 variant (GISAID: EPI_ISL_2779639) was evaluated using a hamster model as

previously descripted[67]. Briefly, hamsters were intranasally inoculated with 1×10^4 PFU/100 μL of SARS-CoV-2 Beta strain. The triple antibody cocktail composed of X01, X10 and X17 in a ratio of 1:1:1 was administrated intraperitoneally at a total dose of 35 mg/kg at 24 hours post-challenge, PBS was used as negative control. The body weight change and health status were recorded daily. Hamsters were euthanized at 6 days post-challenge for detection of viral load in respiratory tract organs and analysis of pathogenesis in lung lobes. The indicators of therapeutic efficacy were including body weight change, tissue viral RNA load, and the histopathology examination score were tested.

SARS-CoV-2 RNA quantification

The tissue samples including lung, trachea and nasal turbinate were separated from infected hamsters and homogenized with TissueLyser II (Qiagen), and SARS-CoV-2 RNA was extracted using the QIAamp Viral RNA Mini Kit ((52906, Qiagen). Then, the viral RNA concentration was quantified using a SARS-CoV-2 RT-PCR Kit (WS-1248, Wantai BioPharm) according to the manufacturer's instructions.

Quantification and statistical analysis

GraphPad Prism (version 8.0.1) was used for all statistical calculations. To compare continuous variables, Mann Whitney test was performed between groups. For statistical difference analysis, P values less than 0.05 were considered statistically significant. ns: not significant; *P <0.05; **P < 0.01; ***P < 0.001. IC_{50} values were calculated by non-linear regression analysis (log(agonist) vs response - Variable slope (four parameters)).

636

637

Acknowledgments: This study was supported by the National Natural Science Foundation of China (81991491 (to N.X.), 31730029 (to N.X.), 32170943 (to T.Z.), 82001756 to T.L.), Fujian Natural Science Foundation for Distinguished Young Scholars (2020J06007 (to T.Z.)), Xiamen Youth Innovation Fund Project (3502Z20206060 (to T.Z)) and the Bill &Melinda Gates Foundation (INV-005834 (to N.X.)).

Author contributions: N.X., T.Z., Q.Z., J.Z. and H.X. designed the study; Y.Z., J.Z., Y.J., M.W. and Y.W. participated in the neutralization assay; L.M., S.Y. and Y.W performed the viral escape assay; J.M., M.Z., L.Y., T.C. and Y.G. designed and performed the therapy experiment in the hamster model; R.F. and M.Y. tested the binding activity; H.S., L.L. and Y.H. prepared the cryo-EM grids and recorded the cryo-EM movies; H.S., T.L. and Q.Z. processed the data and obtained all 3D reconstructions; N.X., T.Z., H.X., R.Q. and S.W. analyzed data; H.X., H.S., S.W. and T.Z. wrote the manuscript; Q.Y., Z.Z., S.L., S.W., T.Z., Y.G., Q.Z. and N.X. participated in the discussion and interpretation of the results. All authors reviewed and approved the paper.

Data availability: The cryo-EM density maps have been deposited in the Electron Microscopy Data Bank (EMDB) with the accession codes of XXX, XXX, XXX, XXX, XXX, and the corresponding atomic coordinates have been deposited in the Protein Data Bank (PDB) with the accession codes of XXX, XXX, XXX, XXX, XXX.

Conflict of interest: The authors declare that they have no conflicts of interest.

References:

1 Zhou, P. *et al.* A pneumonia outbreak associated with a new coronavirus of probable bat origin. *Nature* **579**, 270-273, doi:10.1038/s41586-020-2012-7 (2020).

2 Burki, T. Understanding variants of SARS-CoV-2. *Lancet* **397**, 462, doi:10.1016/S0140-6736(21)00298-1 (2021).

3 Wang, C., Horby, P. W., Hayden, F. G. & Gao, G. F. A novel coronavirus outbreak of global health concern. *Lancet* **395**, 470-473, doi:10.1016/S0140-6736(20)30185-9 (2020).

4 Barnes, C. O. *et al.* SARS-CoV-2 neutralizing antibody structures inform therapeutic strategies. *Nature* **588**, 682-687, doi:10.1038/s41586-020-2852-1 (2020).

5 Ju, B. *et al.* Human neutralizing antibodies elicited by SARS-CoV-2 infection. *Nature* **584**, 115-119, doi:10.1038/s41586-020-2380-z (2020).

6 Tomas, K. K., G. *President Trump Received Experiment Antibody Treatment*, <https://www.nytimes.com/2020/10/02/health/trump-antibody-treatment.html> (2020).

7 An EUA for sotrovimab for treatment of COVID-19. *Med Lett Drugs Ther* **63**, 97-xx98 (2021).

8 An EUA for Bamlanivimab-A Monoclonal Antibody for COVID-19. *JAMA* **325**, 880-881, doi:10.1001/jama.2020.24415 (2021).

9 Casirivimab and imdevimab (REGEN-COV) for post-exposure prophylaxis of COVID-19. *Med Lett Drugs Ther* **63**, 130-131 (2021).

10 Dougan, M. *et al.* Bamlanivimab plus Etesevimab in Mild or Moderate Covid-19. *N Engl J Med* **385**, 1382-1392, doi:10.1056/NEJMoa2102685 (2021).

11 Cao, Y. *et al.* Omicron escape the majority of existing SARS-CoV-2 neutralizing antibodies. *Nature*, doi:10.1038/d41586-021-03796-6 (2021).

12 Cele, S. *et al.* Omicron extensively but incompletely escapes Pfizer BNT162b2 neutralization. *Nature*, doi:10.1038/d41586-021-03824-5 (2021).

13 Baum, A. *et al.* Antibody cocktail to SARS-CoV-2 spike protein prevents rapid mutational escape seen with individual antibodies. *Science* **369**, 1014-+, doi:10.1126/science.abd0831 (2020).

14 Liu, Z. M. *et al.* Identification of SARS-CoV-2 spike mutations that attenuate monoclonal and serum antibody neutralization. *Cell Host Microbe* **29**, 477-+, doi:10.1016/j.chom.2021.01.014 (2021).

15 Weisblum, Y. *et al.* Escape from neutralizing antibodies by SARS-CoV-2 spike protein variants. *Elife* **9**, doi:ARTN e6131210.7554/eLife.61312 (2020).

16 Wang, P. F. *et al.* Antibody resistance of SARS-CoV-2 variants B.1.351 and B.1.1.7. *Nature* **593**, 130-+, doi:10.1038/s41586-021-03398-2 (2021).

17 Hoffmann, M. *et al.* SARS-CoV-2 variants B.1.351 and P.1 escape from neutralizing antibodies. *Cell* **184**, 2384-+, doi:10.1016/j.cell.2021.03.036 (2021).

18 Wang, P. F. *et al.* Increased resistance of SARS-CoV-2 variant P.1 to antibody neutralization. *Cell Host Microbe* **29**, 747-+, doi:10.1016/j.chom.2021.04.007 (2021).

19 Li, Q. Q. *et al.* The Impact of Mutations in SARS-CoV-2 Spike on Viral Infectivity and Antigenicity. *Cell* **182**, 1284-+, doi:10.1016/j.cell.2020.07.012 (2020).

20 Starr, T. N., Greaney, A. J., Dingens, A. S. & Bloom, J. D. Complete map of SARS-CoV-2 RBD mutations that escape the monoclonal antibody LY-CoV555 and its cocktail with LY-CoV016. *Cell Rep Med* **2**, 100255, doi:10.1016/j.xcrm.2021.100255 (2021).

21 Hoffmann, M. *et al.* SARS-CoV-2 Cell Entry Depends on ACE2 and TMPRSS2 and Is Blocked by a Clinically Proven Protease Inhibitor. *Cell* **181**, 271-+, doi:10.1016/j.cell.2020.02.052 (2020).

22 Matheson, N. J. & Lehner, P. J. How does SARS-CoV-2 cause COVID-19? *Science* **369**, 510-511, doi:DOI: 10.1126/science.abc6156 (2020).
23 Wu, Y. *et al.* A noncompeting pair of human neutralizing antibodies block COVID-19 virus binding to its receptor ACE2. *Science* **368**, 1274-+, doi:10.1126/science.abc2241 (2020).
24 Piccoli, L. *et al.* Mapping Neutralizing and Immunodominant Sites on the SARS-CoV-2 Spike Receptor-Binding Domain by Structure-Guided High-Resolution Serology. *Cell* **183**, 1024-+, doi:10.1016/j.cell.2020.09.037 (2020).
25 Cao, Y. L. *et al.* Humoral immune response to circulating SARS-CoV-2 variants elicited by inactivated and RBD-subunit vaccines. *Cell Res* **31**, 732-741, doi:10.1038/s41422-021-00514-9 (2021).
26 Starr, T. N. *et al.* SARS-CoV-2 RBD antibodies that maximize breadth and resistance to escape. *Nature* **597**, 97-102, doi:10.1038/s41586-021-03807-6 (2021).
27 Pinto, D. *et al.* Cross-neutralization of SARS-CoV-2 by a human monoclonal SARS-CoV antibody. *Nature* **583**, 290-295, doi:10.1038/s41586-020-2349-y (2020).
28 Tortorici, M. A. *et al.* Broad sarbecovirus neutralization by a human monoclonal antibody. *Nature* **597**, 103-+, doi:10.1038/s41586-021-03817-4 (2021).
29 Starr, T. N. *et al.* SARS-CoV-2 RBD antibodies that maximize breadth and resistance to escape. *Nature* **597**, 97-+, doi:10.1038/s41586-021-03807-6 (2021).
30 Copin, R. *et al.* The monoclonal antibody combination REGEN-COV protects against SARS-CoV-2 mutational escape in preclinical and human studies. *Cell* **184**, 3949-3961 e3911, doi:10.1016/j.cell.2021.06.002 (2021).
31 Shen, C. *et al.* A multimechanistic antibody targeting the receptor binding site potently cross-protects against influenza B viruses. *Sci Transl Med* **9**, doi:10.1126/scitranslmed.aam5752 (2017).
32 Skowronski, D. M. *et al.* Cross-lineage influenza B and heterologous influenza A antibody responses in vaccinated mice: immunologic interactions and B/Yamagata dominance. *PLoS One* **7**, e38929, doi:10.1371/journal.pone.0038929 (2012).
33 Maroof, A., Yorgensen, Y. M., Li, Y. & Evans, J. T. Intranasal vaccination promotes detrimental Th17-mediated immunity against influenza infection. *PLoS Pathog* **10**, e1003875, doi:10.1371/journal.ppat.1003875 (2014).
34 Xiong, H. L. *et al.* Robust neutralization assay based on SARS-CoV-2 S-protein-bearing vesicular stomatitis virus (VSV) pseudovirus and ACE2-overexpressing BHK21 cells. *Emerg Microbes Infect* **9**, 2105-2113, doi:10.1080/22221751.2020.1815589 (2020).
35 Yuan, M. *et al.* Structural basis of a shared antibody response to SARS-CoV-2. *Science* **369**, 1119-1123, doi:10.1126/science.abd2321 (2020).
36 Yan, R. *et al.* Structural basis for the recognition of SARS-CoV-2 by full-length human ACE2. *Science* **367**, 1444-1448, doi:10.1126/science.abb2762 (2020).
37 Cameroni, E. *et al.* Broadly neutralizing antibodies overcome SARS-CoV-2 Omicron antigenic shift. *Nature*, doi:10.1038/s41586-021-04386-2 (2021).
38 Li, T. *et al.* Cross-neutralizing antibodies bind a SARS-CoV-2 cryptic site and resist circulating variants. *Nat Commun* **12**, 5652, doi:10.1038/s41467-021-25997-3 (2021).
39 Cameroni, E. *et al.* Broadly neutralizing antibodies overcome SARS-CoV-2 Omicron antigenic shift. *Nature*, doi:10.1038/d41586-021-03825-4 (2021).
40 *Update on COVID-19 variants and impact on bamlanivimab distribution.*,

748 <https://Www.Phe.Gov/Emergency/Events/COVID19/Investigation-
749 MCM/Bamlanivimab/Pages/Default.Aspx.> (2021).
750 41 *Update on COVID-19 variants and impact on bamlanivimab distribution*,
751 <Https://Www.Phe.Gov/Emergency/Events/COVID19/Investigation-MCM/Bamlanivimab-
752 Etesevimab/Pages/Default.Aspx> (2021).
753 42 Tortorici, M. A. *et al.* Broad sarbecovirus neutralization by a human monoclonal antibody.
754 *Nature* **597**, 103-108, doi:10.1038/s41586-021-03817-4 (2021).
755 43 Liu, L. *et al.* Striking antibody evasion manifested by the Omicron variant of SARS-CoV-2. *Nature*,
756 doi:10.1038/d41586-021-03826-3 (2021).
757 44 Planas, D. *et al.* Considerable escape of SARS-CoV-2 Omicron to antibody neutralization. *Nature*,
758 doi:10.1038/d41586-021-03827-2 (2021).
759 45 Ku, Z. *et al.* Nasal delivery of an IgM offers broad protection from SARS-CoV-2 variants. *Nature*
760 **595**, 718-723, doi:10.1038/s41586-021-03673-2 (2021).
761 46 Ma, X. *et al.* Nanoparticle Vaccines Based on the Receptor Binding Domain (RBD) and Heptad
762 Repeat (HR) of SARS-CoV-2 Elicit Robust Protective Immune Responses. *Immunity* **53**, 1315-
763 1330 e1319, doi:10.1016/j.immuni.2020.11.015 (2020).
764 47 Hansen, J. *et al.* Studies in humanized mice and convalescent humans yield a SARS-CoV-2
765 antibody cocktail. *Science* **369**, 1010-1014, doi:10.1126/science.abd0827 (2020).
766 48 Lv, Z. *et al.* Structural basis for neutralization of SARS-CoV-2 and SARS-CoV by a potent
767 therapeutic antibody. *Science* **369**, 1505-1509, doi:10.1126/science.abc5881 (2020).
768 49 FDA. *FDA Approves Treatment for Ebola Virus.*, <https://www.fdagov/drugs/drug-safety-and-
769 availability/fda-approves-treatment-ebola-virus> (2020).
770 50 Jette, C. A. *et al.* Broad cross-reactivity across sarbecoviruses exhibited by a subset of COVID-
771 19 donor-derived neutralizing antibodies. *Cell Rep* **36**, 109760,
772 doi:10.1016/j.celrep.2021.109760 (2021).
773 51 Corti, D., Purcell, L. A., Snell, G. & Veesler, D. Tackling COVID-19 with neutralizing monoclonal
774 antibodies. *Cell* **184**, 4593-4595, doi:10.1016/j.cell.2021.07.027 (2021).
775 52 Whitt, M. A. Generation of VSV pseudotypes using recombinant DeltaG-VSV for studies on virus
776 entry, identification of entry inhibitors, and immune responses to vaccines. *J Virol Methods*
777 **169**, 365-374, doi:10.1016/j.jviromet.2010.08.006 (2010).
778 53 Zheng, S. Q. *et al.* MotionCor2: anisotropic correction of beam-induced motion for improved
779 cryo-electron microscopy. *Nature methods* **14**, 331-332, doi:10.1038/nmeth.4193 (2017).
780 54 Zhang, K. Gctf: Real-time CTF determination and correction. *Journal of structural biology* **193**,
781 1-12, doi:10.1016/j.jsb.2015.11.003 (2016).
782 55 Punjani, A., Rubinstein, J. L., Fleet, D. J. & Brubaker, M. A. cryoSPARC: algorithms for rapid
783 unsupervised cryo-EM structure determination. *Nature methods* **14**, 290-296,
784 doi:10.1038/nmeth.4169 (2017).
785 56 Scheres, S. H. & Chen, S. Prevention of overfitting in cryo-EM structure determination. *Nature*
786 *methods* **9**, 853-854, doi:10.1038/nmeth.2115 (2012).
787 57 Kucukelbir, A., Sigworth, F. J. & Tagare, H. D. Quantifying the local resolution of cryo-EM density
788 maps. *Nature methods* **11**, 63-65, doi:10.1038/nmeth.2727 (2014).
789 58 Wrapp, D. *et al.* Cryo-EM structure of the 2019-nCoV spike in the prefusion conformation.
790 *Science* **367**, 1260-1263, doi:10.1126/science.abb2507 (2020).
791 59 Wu, N. C. *et al.* A natural mutation between SARS-CoV-2 and SARS-CoV determines

neutralization by a cross-reactive antibody. *PLoS Pathog* **16**, e1009089, doi:10.1371/journal.ppat.1009089 (2020).

60 Pettersen, E. F. *et al.* UCSF Chimera--a visualization system for exploratory research and analysis. *Journal of computational chemistry* **25**, 1605-1612, doi:10.1002/jcc.20084 (2004).

61 Emsley, P. & Cowtan, K. Coot: model-building tools for molecular graphics. *Acta crystallographica. Section D, Biological crystallography* **60**, 2126-2132, doi:10.1107/S0907444904019158 (2004).

62 Adams, P. D. *et al.* PHENIX: a comprehensive Python-based system for macromolecular structure solution. *Acta crystallographica. Section D, Biological crystallography* **66**, 213-221, doi:10.1107/S0907444909052925 (2010).

63 Chen, V. B. *et al.* MolProbity: all-atom structure validation for macromolecular crystallography. *Acta crystallographica. Section D, Biological crystallography* **66**, 12-21, doi:10.1107/S0907444909042073 (2010).

64 Robert, X. & Gouet, P. Deciphering key features in protein structures with the new ENDscript server. *Nucleic acids research* **42**, W320-324, doi:10.1093/nar/gku316 (2014).

65 Goddard, T. D. *et al.* UCSF ChimeraX: Meeting modern challenges in visualization and analysis. *Protein Sci* **27**, 14-25, doi:10.1002/pro.3235 (2018).

66 Pettersen, E. F. *et al.* UCSF ChimeraX: Structure visualization for researchers, educators, and developers. *Protein Sci* **30**, 70-82, doi:10.1002/pro.3943 (2021).

67 Yuan, L. *et al.* Gender associates with both susceptibility to infection and pathogenesis of SARS-CoV-2 in Syrian hamster. *Signal Transduct Target Ther* **6**, 136, doi:10.1038/s41392-021-00552-0 (2021).

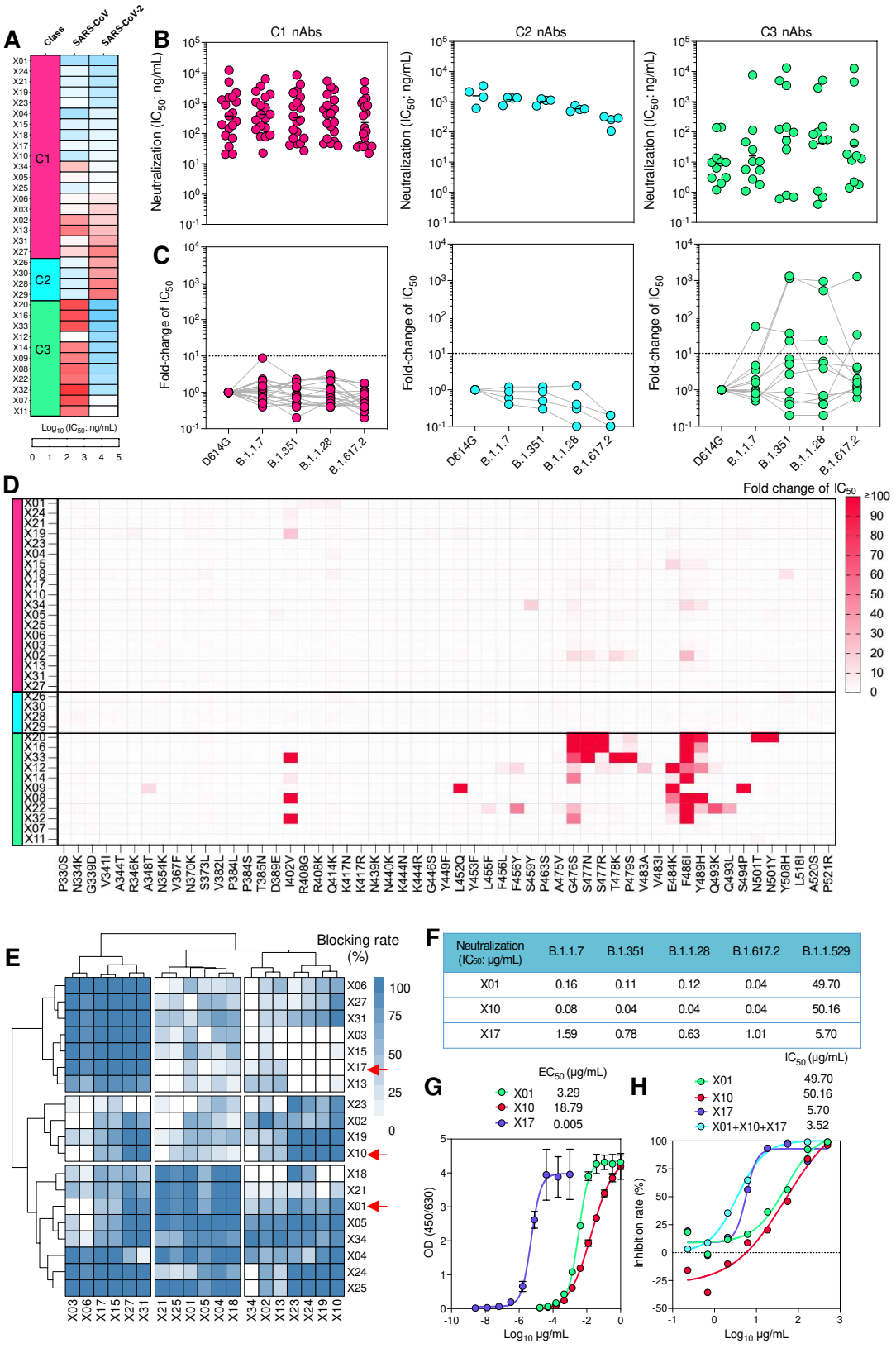

815

816 **Fig. 1. Characterization of broadly neutralizing nAbs induced by sequential**

817 **immunization of pseudoviruses of SARS-CoV and SARS-CoV-2.** (**A**) Classification

818 of a panel of 34 nAbs based on their cross-neutralization of SARS-CoV and SARS-
819 CoV-2. The neutralization potencies of nAbs were evaluated by recombinant VSV-
820 based pseudoviruses of SARS-CoV and SARS-CoV-2. The IC_{50} values ranging from 1
821 ng/mL to 50 μg/mL were represented in blue to red, respectively. nAbs were classified
822 into classes C1, C2 and C3, based on the fold change of IC_{50} values against SARS-
823 CoV-2 related to SARS-CoV (class C1: 0.1-10, class C2: <0.1, and class C3: >10). (**B**
824 and **C**) The IC_{50} values of three classes of nAbs against pseudoviruses of D614G strain
825 and VOCs B.1.1.7, B.1.351, B.1.1.28 and B.1.617.2 (B) and the IC_{50} fold change
826 compared to that of prototyped SARS-CoV-2 (C). nAbs of Classes C1, C2 and C3 are
827 colored in magenta, cyan and green, respectively. The black lines in (B) indicate the
828 geometric means and the black dashed lines in (C) indicate 10 times in fold change.
829 (**D**) Interfere of single point mutations on neutralization potencies of nAbs in classes
830 C1, C2 and C3. The IC_{50} values for different nAbs were determined against VSV
831 pseudovirus carrying SARS-CoV-2 S protein with single residue substations. The fold
832 changes of IC_{50} values of these mutant pseudoviruses (related to D614G control) were
833 calculated. The abscissa shows different mutant residues. (**E**) Cross-blocking matrix
834 for class C1 nAbs. The concentrations of blocking nAbs (row) and detective nAbs
835 (column) were 500 μg /mL and 10 ng/mL, respectively. The intensity of cyan indicates
836 blocking strength ranging from 0% (no blocking, white) to 100% (complete blocking,
837 dark cyan). Red arrows indicate the representative nAbs (X01, X10 and X17). (**F**)
838 Neutralization potencies of X01, X10 and X17 against SARS-CoV-2 VOCs, including
839 B.1.1.7, B.1.1.28, B.1.351, B.1.617.2 and B.1.1.529. (**G** and **H**) Binding activities (G)

and neutralization potencies (H) of X01, X10 and X17 against SARS-CoV-2 Omicron variant. The EC_{50} and IC_{50} values were calculated by Prism software using with non-linear regression (four parameters).

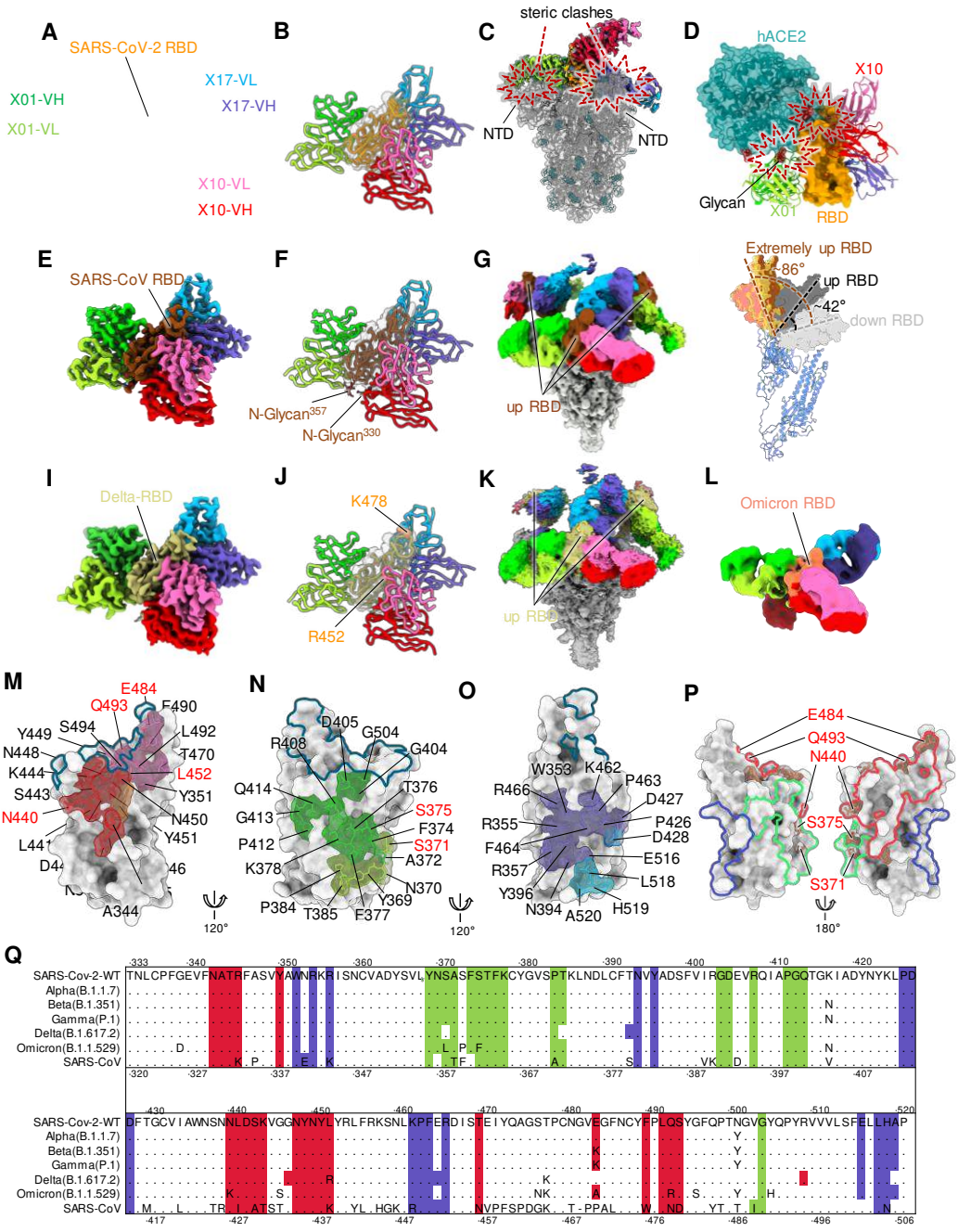

844

845 **Fig. 2. Cryo-EM structures of three-antibody in complex with spike proteins of**
846 **prototyped SARS-CoV-2 and SARS-CoV as well as SARS-CoV-2 Delta and**
847 **Omicron variants.** (**A** and **B**) The domain colored cryo-EM map (A) and cartoon
848 representation (B) of the cryo-EM structure of SARS-CoV-2-S:X10:X01:X17. The
849 surface representation of RBD is shown in transparent. The spike protein was resolved
850 as monomeric form. (**C**) Superimposition of SARS-CoV-2 spike (PDB: 6VSB) into the

density map of SARS-CoV-2-S:X10:X01:X17 indicates the steric clashes (orange dashed boxes) between both Fab X01 and X17 and the neighboring NTD. (**D**) Superimposition of structures of ACE2:RBD (PDB: 6M0J) and SARS-CoV-2-S:X10:X01:X17 shows the steric clashes between both Fab X01 and X10 and ACE2. (**E-G**) Cryo-EM structure of SARS-CoV-S:X10:X01:X17. Local refinement density map of interface (E), original global refinement density map (G) and the cartoon representation (F) of the model were shown. (**H**) The binding of three nAbs on trimeric spike caused the opening of all three RBDs and each RBD showed an extremely opened orientation of ~90° (relative to closed RBD), compared to ~ 42° for the canonical up RBD. (**I-K**) Cryo-EM structure of Delta-S:X10:X01:X17. Local refinement density map of interface (I), original global refinement density map (K) and the cartoon representation (J) of the model were shown. (**L**) The domain colored cryo-EM map of the cryo-EM structure of Omicron-S:X10:X01:X17. (**M-O**) Footprints of X10 (M), X01 (N) and X17 (O) on SARS-CoV-2 WT-RBD. The RBD was presented as surface representation (gray). The residues involved in nAbs interaction were shown as stick representation with transparent surface. The contact regions of the heavy, light chains and both chains of X10 on the RBD were colored in red, pink and brown, respectively. The contact regions of heavy and light chain of X01 were colored in lime and yellow-green, respectively. The contact region of heavy and light chain of X17 were colored in slate blue and sky blue, respectively. The ACE2-binding site (base on PDB no. 7C8D) is marked as the black dotted-line. (**P**) No overlapping of footprints of X10 (red line), X01 (green line) and X17 (slate blue line) was observed on WT-RBD (gray surface

representation). The mutation sites of Omicron variant on RBD are highlighted in coral. (**Q**) Sequence alignment of the RBDs of SARS-CoV-2, VOCs and SARS-CoV with strictly conserved residues shown as dots and the epitopes of three nAbs highlighted with color scheme according to (P).

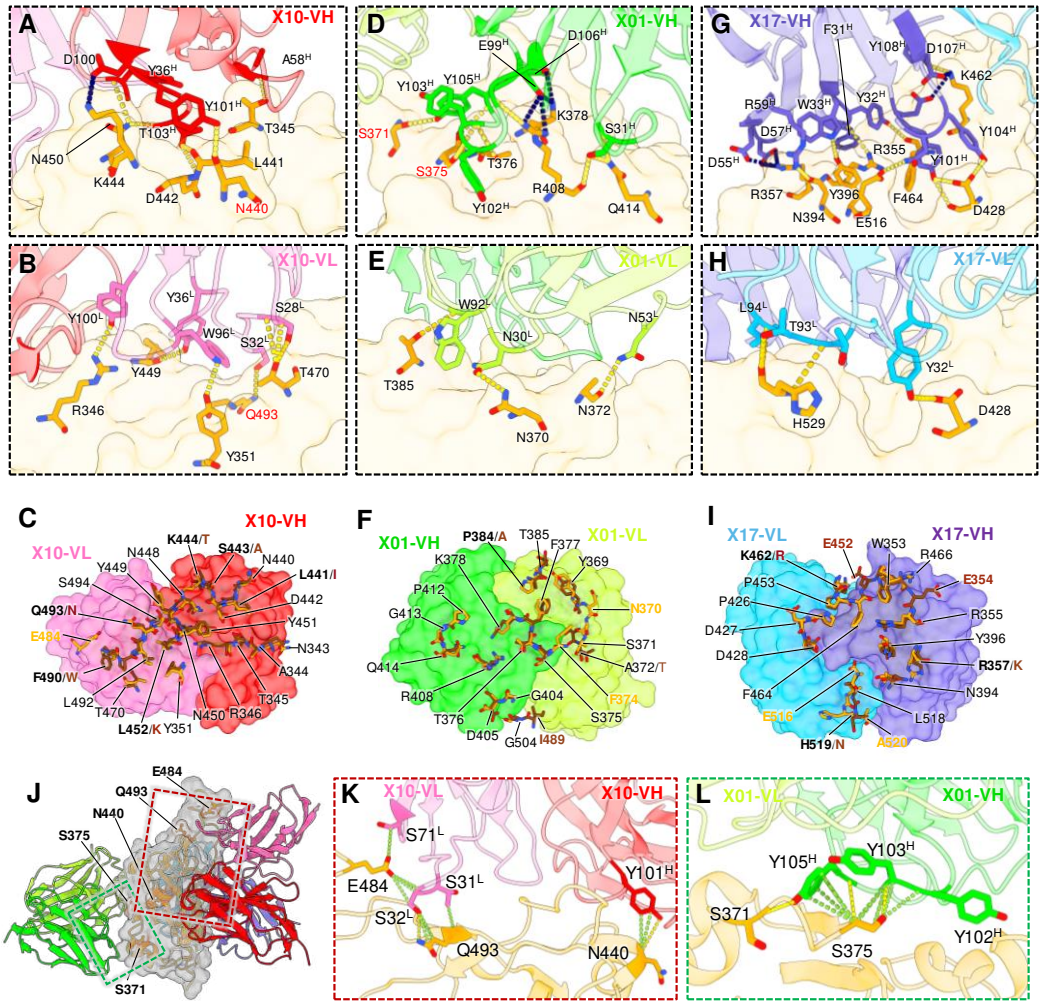

878

879 **Fig. 3. Interactions details of three nAbs and the structural basis of decreased**

880 **neutralization of X10 and X01 against Omicron variant.** (**A** and **B**) Interactions

881 details of SARS-CoV-2 WT-RBD bound by X10. X10 heavy (A) and light chain (B)

882 mediated a network of hydrogen bonds (yellow dash lines) and salt bridges (dark blue

883 dash lines). Models were shown as transparent cartoons and the transparent surface

884 of RBD was also shown, those residues that participated in hydrogen bonds or salt

885 bridges interaction were highlighted and the side chains were shown. (**C**) The structural

886 comparison of X10 epitopes on SARS-CoV-2 (orange stick) and SARS-CoV (brown

887 stick). The VH (red) and VL (pink) of X10 were presented as a transparent surface. (**D**

888 and **E**) Interactions details of SARS-CoV-2 WT-RBD bound by X01 heavy (D) and light
889 chain (E). (**F**) The structural comparison of X01 epitopes on SARS-CoV-2 (orange stick)
890 and SARS-CoV (brown stick). The VH (lime) and VL (yellow-green) of X01 were
891 presented as a transparent surface. (**G** and **H**) Interactions details of SARS-CoV-2 WT-
892 RBD bound by X17 heavy (G) and light chain (H). (**I**) The structural comparison of X17
893 epitopes on SARS-CoV-2 (orange stick) and SARS-CoV (brown stick). The VH (slate
894 blue) and VL (sky blue) of X17 were presented as a transparent surface. Residues on
895 the RBDs involved in the interactions with three nAbs are labeled in black and those
896 diverse residues on epitopes of SARS-CoV and SARS-CoV-2 were highlighted labeled
897 (**J**) The structure of SARS-CoV-2-S:X10:X01:X17 with highlighted residues on WT-
898 RBD regarding to Omicron mutation (displayed in coral stick) that involved in nAbs-
899 RBD interaction. Three Fabs and RBD are shown as cartoon representation with
900 transparent surface. (**K** and **L**) Interaction details of X10 (K) and X01 (L) to those
901 residues that are involved in Omicron mutations. Contacts and hydrogen bonds are
902 marked as green and yellow dash lines, respectively.
903

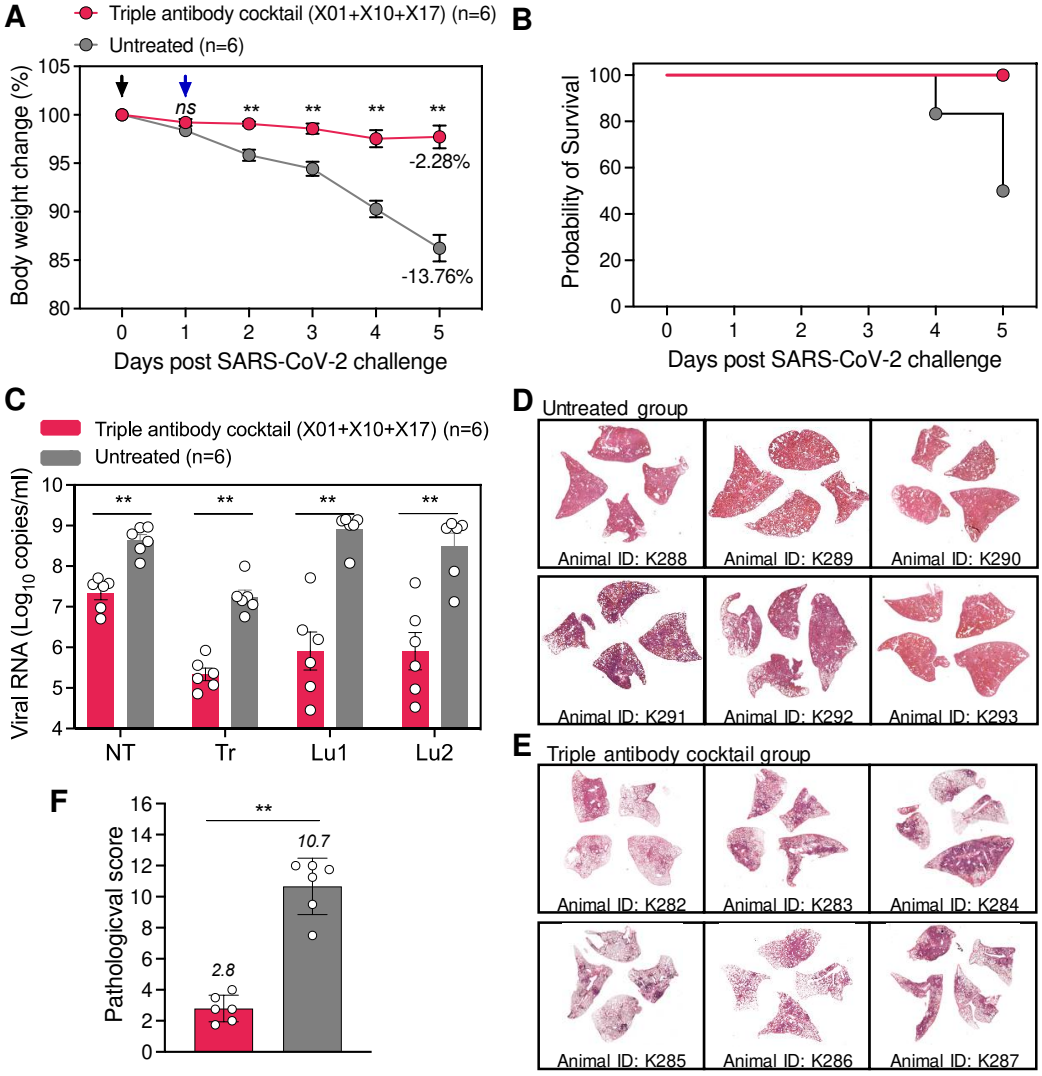

Fig. 4. Efficacy of triple antibody cocktail in protecting against SARS-CoV-2 B.1.351 infection in hamsters. (**A**) Groups of 6 hamsters were intravenously administered (blue arrow) by triple antibody cocktail (1:1:1 mixture of X01, X10 and X17 nAbs) at a total dosage of 35 mg/kg (red) or PBS (gray) as control at one day post B.1.351 intranasal infection (black arrow). Changes in body weight after infection were plotted. The average weight loss of each group at 5 dpi is indicated. Data are means ± SEM. (**B**) Kaplan-Meier survival plot. (**C**) Concentrations of viral RNA in lysates of the nasal turbinate (NT), trachea (Tr) and lung regions proximal (Lu1) and distal (Lu2) to the hilum from hamsters were quantified. Data are shown as means ± SEM. The

difference between the groups was analyzed by Mann Whitney test. (**D** and **E**) H&E-staining of four whole lung lobes collected from the PBS (untreated) group (D) and the triple antibody cocktail treated group (E) at 5 dpi. (**F**) Pathological severity scores for hamster lungs at 5 dpi. The average score of 4 independent lobes is calculated as the pathological severity scores for individual hamsters. Data are shown as means ± SEM. The difference between the groups was analyzed by Mann Whitney test. Asterisks indicate statistical significance (ns: not significant; **: $P < 0.01$).

Supplementary Files

This is a list of supplementary files associated with this preprint. Click to download.

- Supplementaryinformation.pdf
- ValidationreportSARSCoVSX10X01X17.pdf
- ValidationreportSARSCoV2SX10X01X17.pdf
- ValidationreportSARSCoVSX10X01X17interface.pdf
- ValidationreportDeltaSX10X01X17.pdf
- ValidationreportDeltaSX10X01X17interface.pdf
- ValidationreportOmicronSX10X01X17.pdf